H-Plane and E-Plane Loaded Rectangular Slow-Wave Structure for Terahertz TWT Amplifier

Laxma Reddy Billa, Muhammad Nadeem Akram, and Xuyuan Chen

***Abstract*— A novel miniaturized rectangular slow-wave structure (SWS), composed of both H-plane and E-plane corrugations, is proposed for submillimeter or terahertz vacuum electron traveling-wave tube (TWT) devices. The advantage of this SWS is to enhance the interaction impedance, therefore, resulting in higher gain and improved output power of the device. In addition, this structure geometry permits design flexibility to achieve a better dispersion behavior (linear dispersion and wider bandwidth) and easy fabrication by available microfabrication processes. Incorporating an H-plane and E-plane load in the SWS design, we achieved a higher performance TWT amplifier with the central frequency of 400 GHz. Both electromagnetic characteristics and beam–wave interaction analysis are investigated using the 3-D electromagnetic software Computer Simulation Technology studio. The simulation results show that an enhanced interaction of the SWS is obtained, and the amplifier has wide instantaneous bandwidth of 80 GHz and 19.5-dB small signal gain at 400 GHz for 17-kV beam voltage and 20-mA beam current. A saturated output power of more than 19 W is obtained from the large-signal simulations.**

***Index Terms*— H-plane and E-plane loads, slow-wave structure (SWS), terahertz (THz), traveling-wave tube (TWT).**

I. Introduction

THE inherent properties of terahertz (THz) waves enable a wide range of applications, such as imaging, diagnostic systems, advanced radar, communication, and spectroscopy [1]–[5]. The practical applications using THz waves demand high power, wideband, and compact sources. With the advancement in microfabrication technology, vacuum electron traveling-wave tube (TWT) devices for high-power THz sources are the prominent choice over counterparts [6]. In recent years, there has been immense research on the development of the slow-wave structures (SWSs)-based vacuum electronics THz sources [7]–[11].

In submillimeter or THz wave band, the most popular SWS is folded waveguide or serpentine waveguide that can provide a wider bandwidth and moderate output power [12]. However, the complexity of embedded circular beam tunnel in the folded waveguide SWS made it a challenging task to be realized using available microfabrication processes [13], [14]. In contrast, straight rectangular SWSs, such as half-period-staggered double vane [15], sine waveguide [16], trapezoidally corrugated [17], single corrugated waveguide [18], and double corrugated [19], are relatively easy to fabricate and assemble due to the fact that beam tunnel resides as an integral part of structure itself. Mauro and Paloni [8] proposed a double corrugated rectangular SWS to support the circular beam to benefit from the mature circular beam technology in the microwave regime, which can also be realized for the THz band. In [20], a *G*-band TWT amplifier based on a double corrugated SWS was reported, with output power up to 3.7 W, 18-dB gain over frequency range 210–240 GHz for the current density of 226 A/cm^2. A high aspect ratio sheet-beam geometry permits larger beam current compared with a circular beam. A low beam current density mitigates the detrimental space-charge effect and can increase the achievable output power. To utilize the sheet-beam current, half-period-staggered double-vane waveguide, which is a high-aspect-ratio SWS, was proposed for 220-GHz TWT amplifier [21]. Improved versions of this SWS were designed to enhance the performance of device [22], [23]. Furthermore, a half-period-staggered double-vane SWS with different vane geometries, such as rectangular, trapezoidal, sinusoidal, and triangular, was studied using analytical model, multiple modes approximation [10]. Mineo and Paoloni [24] reported that the narrow corrugated SWS provides an effective interaction field compared with the wide corrugated SWS for sheet-beam technology.

The aforementioned straight rectangular SWSs are based on an E-plane metal loaded rectangular waveguide to slow down the phase velocity of the wave into an approximate synchronism with the electron beam. However, they are limited to a relatively low interaction impedance that restricts the gain and output power of the TWT device.

In this paper, we propose an H-plane and E-plane loaded rectangular waveguide as the THz SWS. This novel SWS is designed by incorporating an H-plane metal load in addition to the E-plane metal load in the straight rectangular waveguide. Due to an additional H-plane load, it shows potential benefits, such as an enhanced interaction impedance, thereby higher gain and output power of the device, and flexibility to define the best dispersion curve to be linear for wideband of synchronization. The proposed SWS is designed for 400-GHz central frequency TWT amplifier, and the designed model and para-

Manuscript received December 14, 2015; revised January 30, 2016; accepted February 2, 2016. Date of publication March 7, 2016; date of current version March 22, 2016. This work was supported in part by the Ministry of Education, Norway, under Grant 02079, in part by the Research Council of Norway within the Norwegian Micro - and Nano-Fabrication Facility, NorFab Corporation, under Grant 197411/V30, and in part by the Norwegian Ph.D. Network on Nanotechnology for Microsystems, Nano-Network under Grant 221860/F40. The review of this paper was arranged by Editor M. M. Cahay.

The authors are with the Department of Micro and Nanosystem Technology, University College of Southeast Norway, Borre 3184, Norway (e-mail: laxma.billa@hbv.no; muhammad.n.akram@hbv.no; xuyuan.chen@hbv.no).

Color versions of one or more of the figures in this paper are available online at http://ieeexplore.ieee.org.

Digital Object Identifier 10.1109/TED.2016.2527824

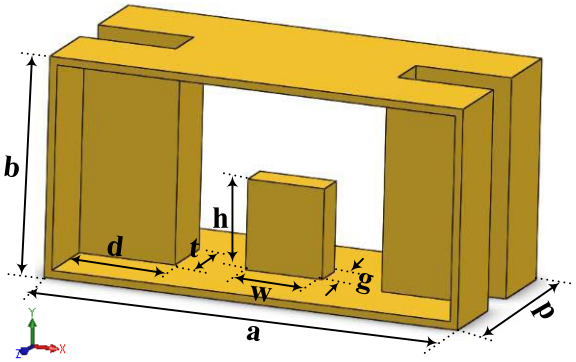

Fig. 1. Schematic design of unit period of the SWS.

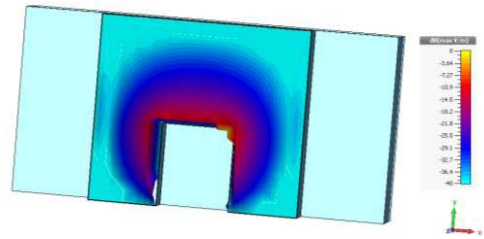

Fig. 2. Fundamental mode axial electric field component on transverse cross section for phase, 2.5π.

meters are described in Section II. The electromagnetic wave properties of the SWS, that is, dispersion curves, interaction impedance, and conductive loss, are reported in Section III. In Section IV, the TWT amplifier performance is simulated by the beam–wave interaction particle-in-cell (PIC) solver. All the simulations are performed using the 3-D electromagnetic commercial software Computer Simulation Technology (CST) studio.

II. Design Description

A schematic is shown in Fig. 1. In our design, a rectangular waveguide consists of periodically repeated two metal corrugations along the longitudinal direction: one is placed on the bottom wall of the broadside of the waveguide width a and the other is on the short side of the waveguide height b. The rectangular waveguide operates in the fundamental mode, i.e., transverse electric (TE_{10}) mode. The metal corrugation, which is on the broader side of waveguide loads the transverse electric field and creates a capacitive loading to the wave, is called an E-plane load. Another metal corrugation, which is on the shorter side of waveguide loads the transverse magnetic field and creates an inductive loading to the wave, is called an H-plane load. Due to the periodic loading, fundamental mode becomes hybrid mode, which supports the slow-wave mode, and the strong axial electric field available above the top surface of E-plane corrugation interacts with the sheet electron beam, as shown in Fig. 2. The corrugation period is p, the E-plane corrugation width, height, and thickness are w, h, and g, respectively, and the H-plane corrugation width, height, and thickness are d, b, and t, respectively.

It is noteworthy that the optimization of device metrics can be done easily using the tailoring of numerous geometry parameters due to both the H-plane and E-plane corrugations.

TABLE I
Design Dimensions of Unit Period of the SWS

Parameters	Dimension(μm)
a	520
b	254
p	240
w	100
g	40
h	113
d	115
t	60

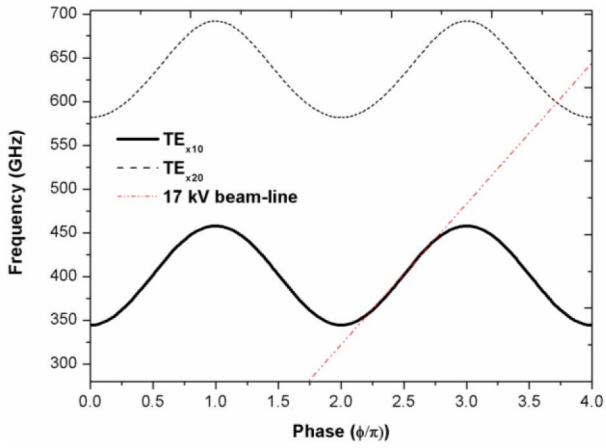

Fig. 3. Dispersion curve for fundamental mode ($TE_{\times 10}$) and second mode ($TE_{\times 20}$).

The chosen SWS transverse dimensions, a and b, are compatible with the standard rectangular waveguide WR-2 cross-sectional dimensions. The period of SWS and corrugation geometry parameters is optimized to achieve a 400-GHz central frequency of operating, linear dispersion curve, and low beam voltage. The design parameters are shown in Table I. This structure can be realized with minimum feature size of available microfabrication process, such as LIGA, DRIE, and computer numerical control nanomilling technique [25].

III. Electromagnetic Wave Properties

To study the electromagnetic wave properties of the combined H-plane and E-plane loaded SWS, a unit period of the SWS is considered. The Floquet boundary condition is imposed on both longitudinal sides of the unit period. On sweeping the phase value of the wave in the unit period, the corresponding frequency and wave field components are obtained with the help of Eigen solver of CST microwave studio.

Fig. 3 shows the dispersion curves of the TE_x fundamental and second modes for defined SWS parameters in Table I. The SWS supports a series of spatial harmonic waves, whose forward spatial harmonic must be chosen as an operational mode for the TWT amplifier. In the fundamental mode, the SWS passband frequency range 345–455 GHz is obtained.

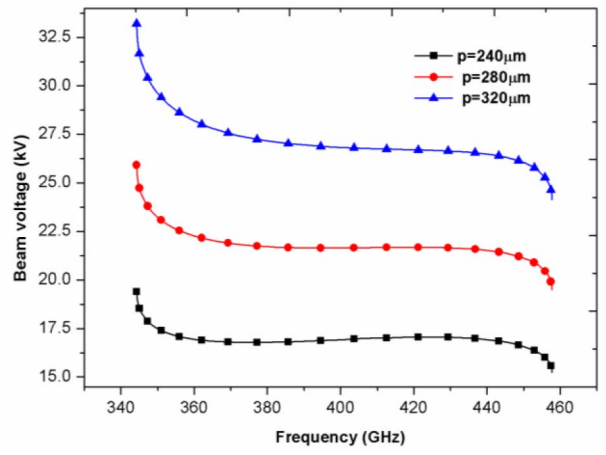

Fig. 4. Beam voltage for varying period p, other parameters kept constant.

In the first forward spatial harmonic (phase, 2.5π–3π), 17-kV beam line intercepts the dispersion curve over 350–440-GHz frequency range. The large instantaneous bandwidth of the TWT amplifier can be predicted from the extremely wide interception in Fig. 3. The synchronous beam voltage to the first harmonic of fundamental wave on varying period length p of the SWS is shown in Fig. 4. For defined design parameters, the constant beam voltage is achieved over a wideband to synchronize with the wave for the beam–wave interaction. Moreover, it is observed that beam voltage decreases on decreasing the length of the period.

One important aim of the SWS is to maximize the interaction impedance, which is a quantitative parameter of the effectiveness of the beam–wave interaction. The larger is the interaction impedance of the SWS, higher will be the gain and the output power of the device. The interaction impedance of the nth spatial harmonic is given by

$$K_{cn} = \frac{\int_S |E_{zn}|^2}{2\beta_n^2 P_{wg}} \tag{1}$$

where E_{zn} is the nth spatial harmonic longitudinal electric field coefficient, β_n is the nth spatial harmonic wave number, P_{wg} is the average power in the cross section, and S is the area of beam cross section. Depending on the available interaction field intensity, geometry parameters for the sheet-beam cross section is optimized to 100 μm $\times$ 60 μm, and positioned 40 μm above the E-plane corrugation. The potential of H-plane load on the structure performance, particularly on interaction impedance, is investigated by varying the H-plane corrugation parameters, d and t, as shown in Fig. 5. The interaction impedance is evaluated for defined sheet-beam parameters in the forward wave first harmonic of the fundamental model. It is interesting to observe the increase in the interaction impedance on increasing both d and t individually with reduced passband range. Hence, it is inferred that the H-plane load enhances the interaction impedance, thereby resulting in higher gain and output power of the device, albeit at reduced operational bandwidth.

It is important to study the conductive losses in the SWS, since in the THz regime, the skin depth of wave is in the order of hundreds of nanometers. Practically, it is very difficult to achieve perfectly smooth metal walls in microfabrication. Considering the surface roughness of the metal wall, the wave undergoes severe attenuation that is critical to minimize to achieve the desired power and gain. The effective conductivity of metal as a function of surface roughness is calculated by [26]

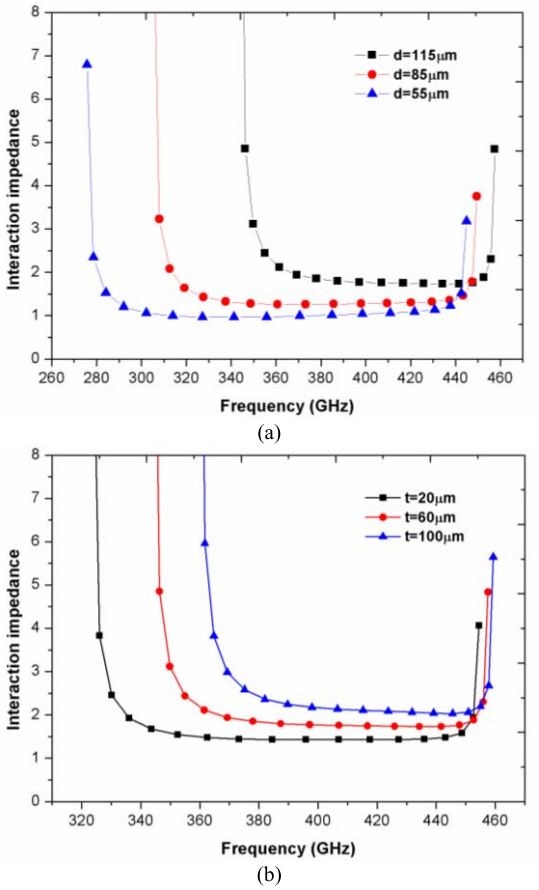

Fig. 5. Interaction impedance for varying H-plane corrugation dimensions. (a) Width d. (b) Thickness t.

$$\sigma_{\text{eff}} = \frac{\sigma}{\left(1 + \exp\left(-\left(\frac{\delta}{2R_q}\right)^{1.6}\right)\right)^2} \tag{2}$$

where δ is the skin depth, R_q is the rms surface roughness, and σ is the conductivity of the pure metal. The effective conductive of the metal is calculated for assumed different surface roughness. Fig. 6 shows the conductive loss in dB/period, which is computed by $\alpha = \omega/(2QV_g)$, where ω is the eigen frequency, and Q and V_g are the perturbed Q-factor and group velocity, respectively. It can be observed that the higher the surface roughness, the larger the conductive loss, which is increased up to 50% for 65-nm surface roughness with respective to the ideal smooth metal wall.

IV. Beam–Wave Interaction

From the known electromagnetic behavior in Section III, such as dispersion, beam voltage, improved interaction impedance, and losses of the interaction structure, the prediction of TWT amplifier performance is carried out with

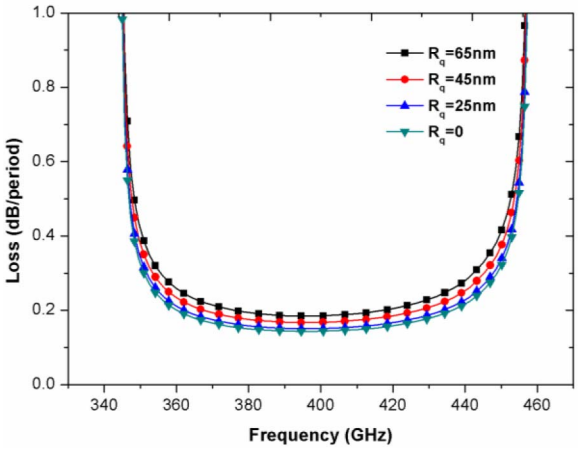

Fig. 6. Loss in dB/period for different values of surface roughness.

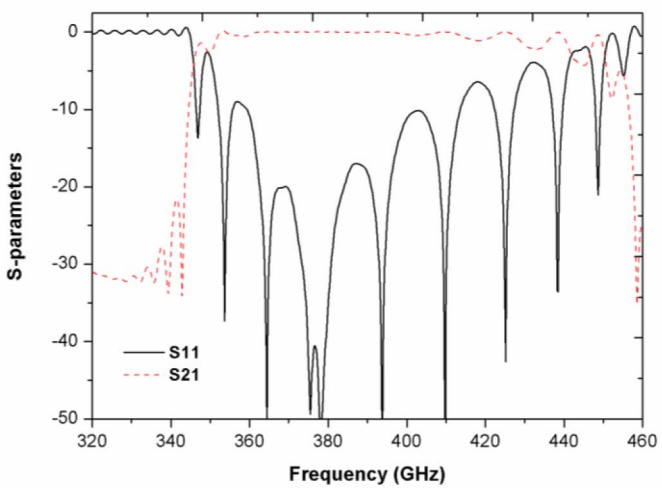

Fig. 8. S-parameters of interaction structure with input and output couplers.

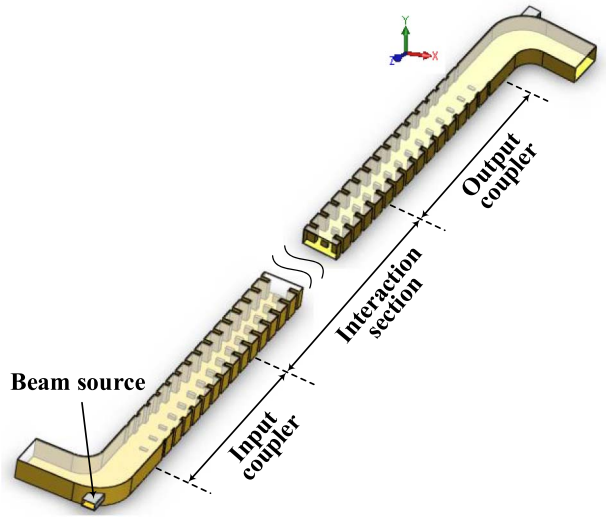

Fig. 7. Schematic of H-plane and E-plane loaded SWS-based TWT amplifier.

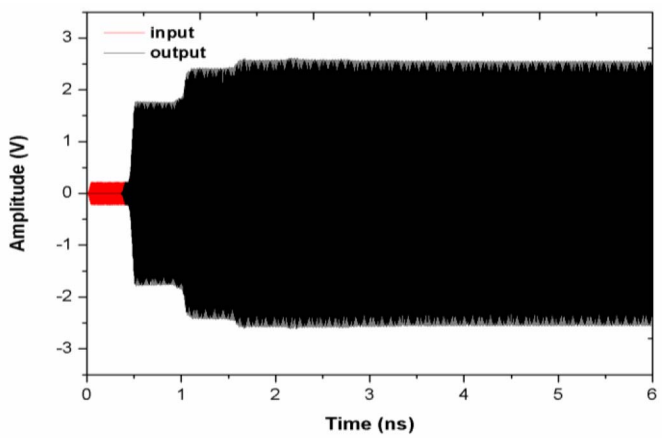

Fig. 9. Input and output signals for 400-GHz CW excitation with 50-mW power.

PIC solver, CST studio. The beam–wave schematic model of TWT amplifier is shown in Fig. 7. We adopted 90 periods in the interaction structure giving the length of 21.6 mm. In order to minimize the reflection from the input port and the output port, and to make it compatible with wave transition between the fast wave and the slow wave, input and output couplers are implemented with 19 periods with vertical tapering of E-plane corrugation height and horizontal tapering of H-plane corrugation width. The reflection (S_{11}) and transmission (S_{21}) coefficients of the complete interaction structure with couplers show good wave propagation characteristics over the passband frequency range, as shown in Fig. 8. To avoid complexity of the simulation model, the electron gun is simplified by setting up a beam-emitting surface as the beam source with 17-kV beam voltage and 20-mA beam current. The beam current is optimized based on the cross section of the beam, and to mitigate the space-charge effect. To confine the beam motion along the propagation path, a uniform magnetic focus of 0.6 T is imposed longitudinally. The calculated effective conductivity $3.6 \times 10^7\ \Omega^{-1}\mathrm{m}^{-1}$ of metal with the assumption of 65-nm surface roughness is defined as the real conductivity of metal walls. The assumed surface roughness can be achieved using available microfabrication technology. Typically, the 3-D PIC simulation of beam–wave interaction consumes more computer resources and takes longer simulation time. Therefore, mesh optimization was performed with respect to the longitudinal electric field. The setup model has 3.1 million mesh cells and 57×10^6 particles at the end of the run.

The small signal gain calculation of the proposed TWT amplifier is performed for the applied Continuous wave (CW) excitation signal of 50-mW input power. Fig. 9 shows the input and output signals at 400-GHz excitation. A stable output signal is observed after 2 ns with gain 19.5 dB and 4.6-W output power. Using an E5530 Xeon processor @2.8 GHz, 72 GHz memory, the computation time is 73 h for 6-ns simulation. To predict the instantaneous bandwidth of the amplifier, the simulations are performed at discrete frequency points over the passband for each simulation run. Fig. 10 shows that an instantaneous bandwidth of 80 GHz in the frequency range 355–435 GHz is achieved. The gain drop in the lower and upper cutoff frequency passband is due to the wave reflections from the

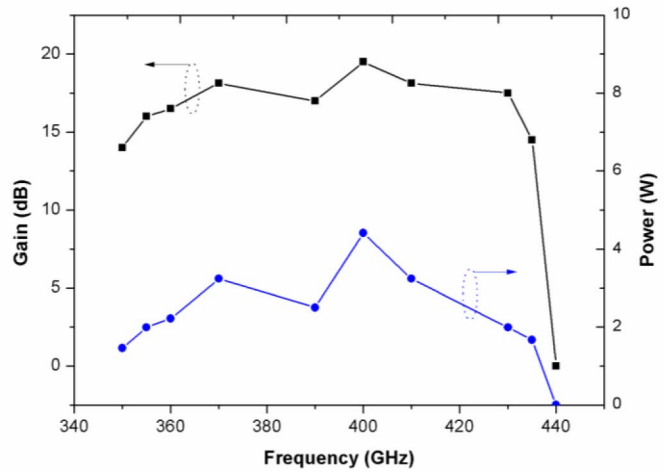

Fig. 10. Gain and output power versus CW excitation frequency of 50 mW.

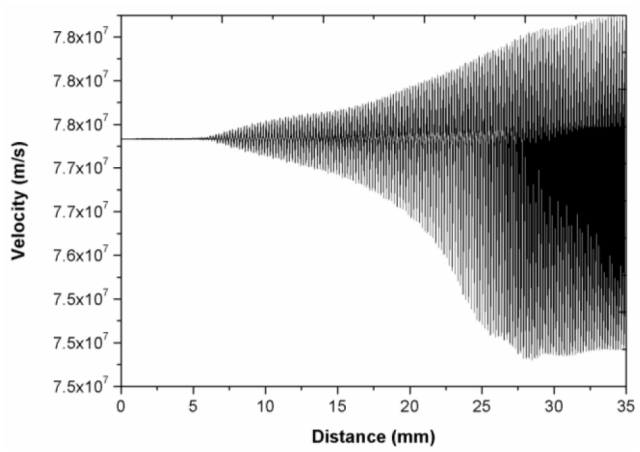

Fig. 11. Beam velocity as a function of the SWS length for 400 GHz.

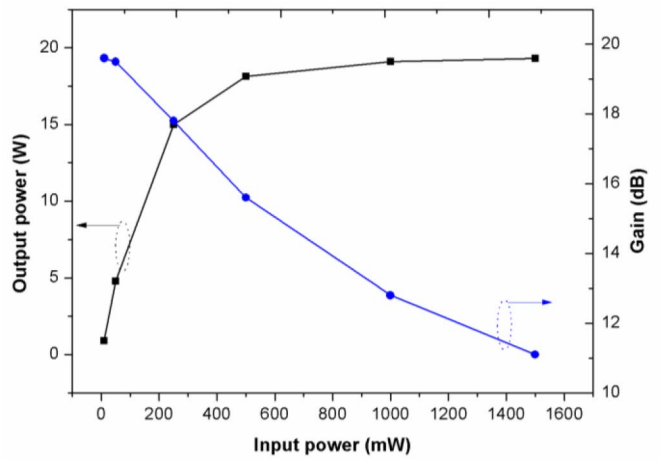

Fig. 12. Output power and gain versus input power of 400-GHz CW.

input and output ports as well as a loss of beam synchronism. An efficiency of more than 0.9% is obtained over the instantaneous bandwidth. The electron velocity as a function of SWS length is shown in Fig. 11. As the beam moves along the propagation direction, the continuous interaction between the beam and the wave causes a decrease in the velocity of bunched beam resulting in nonsynchronization between the beam and the wave at the very end of the tube. A velocity tapering technique can resynchronize the velocity between the beam and the wave, which can help to enhancing the overall beam–wave interaction efficiency. Large signal simulation was also conducted for elevated input power levels of 400-GHz excitation, as shown in Fig. 12. The output power saturates to approximately 19.3 W due to the nonlinear behavior of such devices.

V. Conclusion

The H-plane and E-plane loaded slow-wave circuit has been demonstrated as a novel SWS for 400-GHz central frequency TWT amplifier. Interestingly, an enhanced interaction impedance has been obtained by employing the H-plane load in addition to the usual E-plane load in the SWC. Given the flexibility in numerous design parameters, the SWS gives linear dispersion curve that has wide synchronism with the beam line. The beam–wave interaction simulations have shown promising TWT amplifier performance, such as 80-GHz instantaneous bandwidth, maximum gain of 19.5 dB at 400 GHz for a defined moderate beam voltage of 17 kV and 20-mA beam current. The large signal simulations predicted saturated output power of 19.3 W for 400-GHz CW excitation. The proposed structure topology and geometry parameters are well compatible with feature size of recent microfabrication technologies. Based on the simulation results, the demonstrated performance of the present SWS makes it a suitable candidate for TWT devices.

References

[1] W. E. Baughman, H. Yokus, S. Balci, D. S. Wilbert, P. Kung, and S. M. Kim, "Observation of hydrofluoric acid burns on osseous tissues by means of terahertz spectroscopic imaging," *IEEE Trans. Terahertz Sci. Technol.*, vol. 3, no. 4, pp. 387–394, Jul. 2013.

[2] T. Kleine-Ostmann *et al.*, "Field exposure and dosimetry in the THz frequency range," *IEEE Trans. Terahertz Sci. Technol.*, vol. 4, no. 1, pp. 12–25, Jan. 2014.

[3] K. B. Cooper, R. J. Dengler, N. Llombart, B. Thomas, G. Chattopadhyay, and P. H. Siegel, "THz imaging radar for standoff personnel screening," *IEEE Trans. Terahertz Sci. Technol.*, vol. 1, no. 1, pp. 169–182, Sep. 2011.

[4] J. Federici and L. Moeller, "Review of terahertz and subterahertz wireless communication," *J. Appl. Phys.*, vol. 107, no. 11, pp. 111101-1–111101-22, Jun. 2010.

[5] J. Qin, Y. Ying, and L. Xie, "The detection of agricultural products and food using terahertz spectroscopy: A review," *Appl. Spectrosc. Rev.*, vol. 48, no. 6, pp. 439–457, 2013.

[6] J. H. Booske *et al.*, "Vacuum electronic high power terahertz sources," *IEEE Trans. Terahertz Sci. Technol.*, vol. 1, no. 1, pp. 54–75, Sep. 2011.

[7] Y.-M. Shin and L. R. Barnett, "Intense wideband terahertz amplification using phase shifted periodic electron-plasmon coupling," *Appl. Phys. Lett.*, vol. 92, no. 9, pp. 091501-1–091501-3, Mar. 2008.

[8] M. Mineo and C. Paoloni, "Double-corrugated rectangular waveguide slow-wave structure for terahertz vacuum devices," *IEEE Trans. Electron Devices*, vol. 57, no. 11, pp. 3169–3175, Nov. 2010.

[9] M. Sumathy, K. J. Vinoy, and S. K. Datta, "Analysis of ridge-loaded folded-waveguide slow-wave structures for broadband traveling-wave tubes," *IEEE Trans. Electron Devices*, vol. 57, no. 6, pp. 1440–1446, Jun. 2010.

[10] W. Xie, Z.-C. Wang, J. Luo, and Q. Liu, "Theory and simulation of arbitrarily shaped groove staggered double grating array waveguide," *IEEE Trans. Electron Devices*, vol. 61, no. 6, pp. 1707–1714, Jun. 2014.

[11] M. Zhang *et al.* "A modified slow-wave structure for backward-wave oscillator design in THz band," *IEEE Trans. Terahertz Sci. Technol.*, vol. 4, no. 6, pp. 741–748, Nov. 2014.

[12] M. A. Basten, J. C. Tucek, D. A. Gallagher, K. E. Kreischer, and R. Mihailovich, "A 0.85 THz vacuum-based power amplifier," in *Proc. 13th IEEE IVEC*, Apr. 2012, pp. 39–40.
[13] C. D. Joye *et al.*, "Demonstration of a high power, wideband 220-GHz traveling wave amplifier fabricated by UV-LIGA," *IEEE Trans. Electron Devices*, vol. 61, no. 6, pp. 1672–1678, Jun. 2014.
[14] K. T. Nguyen *et al.*, "Design methodology and experimental verification of serpentine/folded-waveguide TWTs," *IEEE Trans. Electron Devices*, vol. 61, no. 6, pp. 1679–1686, Jun. 2014.
[15] Y.-M. Shin, L. R. Barnett, D. Gamzina, N. C. Luhmann, Jr., M. Field, and R. Borwick, "Terahertz vacuum electronic circuits fabricated by UV lithographic molding and deep reactive ion etching," *Appl. Phys. Lett.*, vol. 95, no. 18, pp. 181505-1–181505-3, Nov. 2009.
[16] X. Xu *et al.*, "A watt-class 1-THz backward-wave oscillator based on sine waveguide," *Phys. Plasmas*, vol. 19, no. 1, 2012, Art. ID 013113.
[17] M. R. Amin, K. Ogura, J. Kojima, and R. H. Sagor, "Electromagnetic properties of a trapezoidally corrugated slow wave structure for backward wave oscillators," *IEEE Trans. Plasma Sci.*, vol. 42, no. 6, pp. 1495–1501, Jun. 2014.
[18] C. D. Joye, J. P. Calame, A. M. Cook, and M. Garven, "High-power copper gratings for a sheet-beam traveling-wave amplifier at G-band," *IEEE Trans. Electron Devices*, vol. 60, no. 1, pp. 506–509, Jan. 2013.
[19] C. Paoloni *et al.*, "Design and realization aspects of 1-THz cascade backward wave amplifier based on double corrugated waveguide," *IEEE Trans. Electron Devices*, vol. 60, no. 3, pp. 1236–1243, Mar. 2013.
[20] C. Paoloni and M. Mineo, "Double corrugated waveguide for G-band traveling wave tubes," *IEEE Trans. Electron Devices*, vol. 61, no. 12, pp. 4259–4263, Dec. 2014.
[21] Y.-M. Shin, A. Baig, L. R. Barnett, N. C. Luhmann, Jr., J. Pasour, and P. Larsen, "Modeling investigation of an ultrawideband terahertz sheet beam traveling-wave tube amplifier circuit," *IEEE Trans. Electron Devices*, vol. 58, no. 9, pp. 3213–3218, Sep. 2011.
[22] J. Lai *et al.*, "W-band 1-kW staggered double-vane traveling-wave tube," *IEEE Trans. Electron Devices*, vol. 59, no. 2, pp. 496–503, Feb. 2012.
[23] X. Shi*et al.*, "Study on wideband sheet beam traveling wave tube based on staggered double vane slow wave structure," *IEEE Trans. Plasma Sci.*, vol. 42, no. 12, pp. 3996–4003, Dec. 2014.
[24] M. Mineo and C. Paoloni, "Narrow corrugation rectangular waveguide for terahertz TWTs," *Electron. Lett.*, vol. 46, no. 13, pp. 927–928, Jun. 2010.
[25] Y.-M. Shin, A. Baig, R. Barchfeld, D. Gamzina, L. R. Barnett, and N. C. Luhmann, Jr., "Experimental study of multichromatic terahertz wave propagation through planar micro-channels," *Appl. Phys. Lett.*, vol. 100, no. 15, pp. 154103-3–154103-4, Apr. 2012.
[26] R. Zheng and X. Chen, "Parametric simulation and optimization of cold-test properties for a 220 GHZ broadband folded waveguide traveling-wave tube," *J. Infr., Millim. Terahertz Waves*, vol. 30, no. 9, pp. 945–958, Sep. 2009.

Laxma Reddy Billa received the bachelor's degree in electronics and communication engineering from Jawaharlal Nehru technological University, India, in 2010, and the master's degree in electronics engineering from Pondicherry University, India, in 2013. He is currently pursuing the Ph.D. degree with the Department of Micro- and Nanosystem Technology, University College of Southeast Norway.

Muhammad Nadeem Akram was born in Pakistan in 1971. He received the B.Sc. degree in electrical engineering from University of Engineering and Technology, Lahore, Pakistan, in 1994, and the Ph.D. degree from the KTH Royal Institute of Technology, Stockholm, Sweden, in 2005.

He has been an Associate Professor with the University College of Southeast Norway, since 2007. His current research interests are integrated optics, semiconductor laser modeling, imaging optics, laser projectors, speckle reduction, and terahertz device technology.

Xuyuan Chen received the B.Sc. degree in semiconductor physics from Northwest University, China, in 1983, the M.Eng. degree in electrical engineering from Xi'an Jiaotong University, China, in 1988, and the Ph.D. degree in semiconductor materials and devices from the Eindhoven University of Technology, The Netherlands, in 1997.

Since 2004, he has been a Professor with the University College of Southeast Norway.